Computational Structural Engineering
An International Journal
Vol. 1, No. 2, pp. 107~116 (2001)

Computational Structural Engineering Institute

Finite Element Analysis of Reinforced Concrete Shear Walls with a Crack under Cyclic Loading

S. Kato[1], M. Ohya[†], S. Shimaoka,[1] and M. Takayama[2]

[1]*Dept. of Architecture and Civil Engrg, Toyohashi Univ. of Tech.,1-1 Tempaku, Toyohashi, 441-8580, Japan*
[†]*Tech. Development Center, Toyohashi Univ. of Tech.,1-1 Tempaku, Toyohashi, 441-8580, Japan*
[2]*Dept. of Architecture, Kanazawa Institute of Tech., 7-1 Ohgigaoka, Nonoichi, Ishikawa, 921-8501, Japan*

Received August 2001; Accepted December 2001

ABSTRACT

The present paper investigates the nonlinear behavior of reinforced concrete shear walls with a crank based on a finite element analysis. The loading type is a horizontal cyclic one such as earthquake loads. Experiments of the shear walls with and without cranks, performed previously to see how the behavior changes depending on the crank, are compared with the results obtained from the finite element analysis. The finite element analysis is based on an isoparametric degenerated shell formulation. The nonlinear constitutive equations for concrete are modeled adopting the formulation based on a concept of Ring Typed-Lattice Model. The experiments indicate that the shear walls with a crank have low stiffness and relatively low carrying capacity compared with an ordinary plane shear wall without cranks and that they are more ductile, and the tendency is also confirmed based on the finite element analysis. Moreover, a good agreement between the experiments and analyses is obtained, accordingly, it is confirmed that the present numerical analysis scheme based on the Lattice Model is a powerful one to evaluate the behavior of reinforced concrete shear walls with cranks and without cranks.

Key words: RC shear wall, crank, lattice model, constitutive law, FEM, cyclic load, nonlinear analysis

1. Introduction

A system of reinforced concrete (RC) shear walls is well known as one of the most significant elements of architectural structures to resist against earthquakes. The structures are thin and are subjected to cyclic loading such as earthquake loadings. A crank typed shear wall, which has a crank within the plan and is one of the spatial shear walls like folded walls or plates, is often used as a partitioning wall in buildings of apartment house and hotels. Such a spatial shear wall seems to have different structural characteristics from those of a usual plane shear wall, because it is subjected to the stresses of out-of-plane due to its shape as described in the previous paper (Takayama, 1990). Despite of crank typed walls being often adopted, there have been few investigations on the crank typed shear walls (Takayama *et al.*, 2000).

The present paper aims, first, at a finite element analysis of crank typed shear walls under cyclic loading. The shear walls analyzed in the paper are the walls to which experiments were performed previously by the fourth author using crank typed shear walls (Takayama *et al.*, 2000). The constitutive equations in the finite element are based on Ring Typed-Lattice Model (Lattice Model) (Kato *et al.*, 1996,1997,1998), which was applied also in the previous researches to analysis of RC structures subjected to cyclic loading. Second, from the comparison between the experiments and analysis, this study aims to show the extensive applicability of the constitutive equations based on Lattice Model, and finally, investigates in detail the structural behavior RC shear walls with a crank subjected to cyclic horizontal loading.

2. Numerical Procedure

In the present numerical analysis of crank typed shear walls, an isoparametric degenerated shell element is applied with an additional use of the nine-node Heterosis element (Hinton *et al.*, 1984). In the element, quadratic

† Corresponding author
Tel.: +81-532446965; Fax: +81-532446831
E-mail address: ohya@st.tutrp.tut.ac.jp

shape functions are used to describe the element geometry. Each node on the sides and corners has three translational and two rotational degrees of freedom, while the central ninth node has only two rotational degrees of freedom. The selective integration rule (Hinton *et al.*, 1984) is used; the 3×3 rule for evaluating the bending stiffness components and the 2×2 rule for the shear stiffness components within a layer in the thickness. To represent the strains in the element, Green Lagrange strain definitions are used. The geometric and material nonlinearities are taken into account. A layered approach is used to describe the material nonlinearities through thickness. Eight layers for concrete elements and two layers for steel reinforcements are assumed.

2.1 Material Behavior of Concrete

A two dimensional concrete element is replaced by the Lattice Model composed of a set of many straight bar elements as shown in Fig. 1 and the detail for the formulation of the Lattice Model is abbreviated here since the detail was explained in the previous paper (Kato *et al.*, 1996, 1997, 1998). The Lattice Model is composed of four hub struts (*a–d*) and eight ring elements (*e–l*). A ring element is composed of four struts (one horizontal, one vertical and two bracing struts), placed like a circular ring. Both ends of each strut are pin-joined to a rigid body. The material characteristics of these struts should be evaluated so that the total behavior of a Lattice Element coincides with a two-dimensional concrete element. In implementation to the FEM, the Lattice Model is located at every integration point and the internal stresses are evaluated as the combination of the simple stress-strain relationship of all the struts.

2.1.1 Constitutive Equations

In Fig. 1, the incremental axial strains $\Delta\varepsilon_i$ of hub strut i (*a–d*) are expressed by Eq.(1) using the incremental strains $(\Delta\varepsilon_X, \Delta\varepsilon_Y, \Delta\gamma_{XY})$ defined with respect to local X and Y coordinate system.

$$\Delta\varepsilon_i = S_{iX}\Delta\varepsilon_X + S_{iY}\Delta\varepsilon_Y + (S_{iXY} + S_{iYK})\frac{\Delta\gamma_{XY}}{2} \tag{1}$$

where θ_i is defined in Fig. 1, for example, as $\theta_a = -45°$ for the hub strut a., and

$$\Delta\varepsilon_X = \frac{\partial\Delta U}{\partial X}, \Delta\varepsilon_Y = \frac{\partial\Delta V}{\partial\Delta Y}, \ \Delta\varepsilon_{XY} = \Delta\varepsilon_{YX} = \frac{\Delta\gamma_{XY}}{2}$$

$$\Delta\gamma_{XY} = \frac{\partial\Delta V}{\partial X} + \frac{\partial\Delta U}{\partial Y}, \ S_{iX} = \cos^2\theta_i$$

$$S_{iY} = \sin^2\theta_i, S_{iXY} = S_{iYX} = \sin\theta_i\cos\theta_i$$

Incremental strains $\Delta\varepsilon_j$ and incremental shear strains $\Delta\gamma_j$ of a ring element $j(e–l)$ shown in Fig. 1 are represented as follows when x_j axis is defined as an axial direction of a horizontal strut for ring element j, and y_j axis as an orthogonal direction as shown in Figs. 2(a) and (b).

$$\Delta\varepsilon_j = S_{jX}\Delta\varepsilon_X + S_{jY}\Delta\varepsilon_Y + (S_{jXY} + S_{jYX}) = \frac{\Delta\gamma_{XY}}{2} \tag{2}$$

$$\Delta\gamma_j = T_{jX}\Delta\varepsilon_X + T_{jY}\Delta\varepsilon_Y + (T_{jXY} + T_{jYX}) = \frac{\Delta\gamma_{XY}}{2} \tag{3}$$

where θ_j for a ring element is defined in Fig. 1, for example, as $\theta_e = 22.5°$ for the ring element ***e***.

$$S_{jX} = \cos^2\theta_j, S_{jY} = \sin^2\theta_j, S_{jXY} = S_{jYX} = \sin\theta_j\cos\theta_j,$$

$$T_{jX} = -\sin\theta_j\cos\theta_j, T_{jY} = \sin\theta_j\cos\theta_j,$$

$$T_{jXY} = \cos^2\theta_j, \ T_{jYX} = -\sin^2\theta_j$$

Due to the incremental strains $\Delta\varepsilon_j$ and $\Delta\gamma_j$, the ring element deforms as shown in Figs. 2(a) and (b). Accordingly, the incremental strains in each strut of H, V, B_1, B_2 in a ring

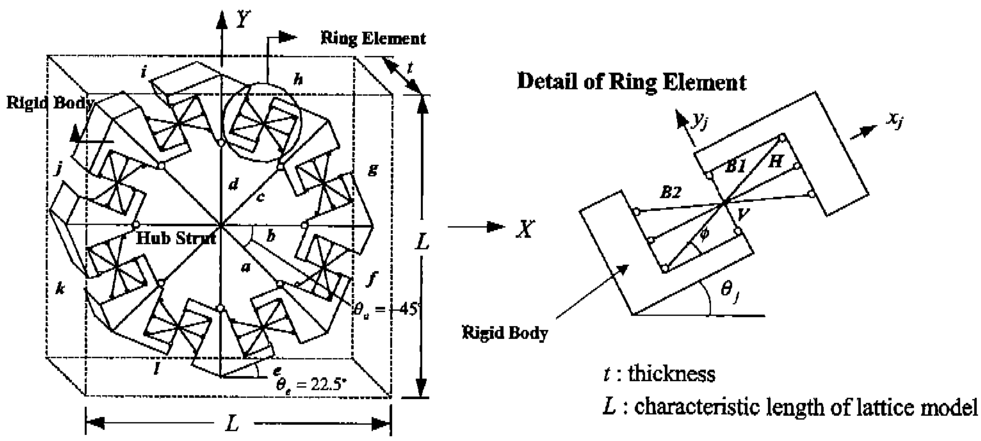

Fig. 1. Ring Typed-Lattice Model.

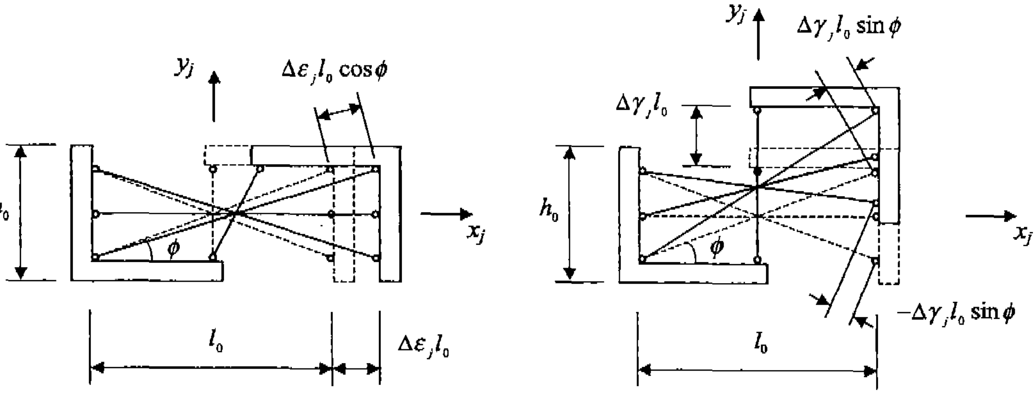

(a) Elongation $\Delta\varepsilon_j$ (b) Shear $\Delta\gamma_j$

Fig. 2. Deformation of Ring Element *j*.

element are obtained as follows.

$$\Delta\varepsilon_j^H = \Delta\varepsilon_j \tag{4}$$

$$\Delta\varepsilon_j^V = \frac{1}{\tan\phi}\Delta\gamma_j \tag{5}$$

$$\Delta\varepsilon_j^{B_1} = \cos^2\phi\Delta\varepsilon_j + \sin\phi\cos\phi\Delta\gamma_j \tag{6}$$

$$\Delta\varepsilon_j^{B_2} = \cos^2\phi\Delta\varepsilon_j - \sin\phi\cos\phi\Delta\gamma_j \tag{7}$$

For instance, the stress σ_i for *i*-th hub strut after increment strains is expressed as follows.

$$\sigma_i = \eta_i\overline{Er}\Delta\varepsilon_i + \sigma_{i0} \tag{8}$$

where $\overline{Er}$, σ_{i0} and η_i are respectively the equivalent stiffness, initial stress and stiffness modification coefficient for each strut at the stage of ε_i before increments. The sum of the virtual strain energy δU_L stored in the Lattice Model is expressed using the virtual strain $\Delta\varepsilon$ for each strut as follows.

$$\begin{aligned}\delta U_L = &\sum_{i=a}^{d}(\eta_i\overline{Er}\Delta\varepsilon_i + \sigma_{i0})\delta\varepsilon_i \\ &\sum_{j=e}^{l}[(\eta_j^H\overline{Er^H}\Delta\varepsilon_{j0}^H + \sigma_{j0}^H)\delta\varepsilon_j^H \\ &+(\eta_j^V\overline{Er^{BV}}\Delta\varepsilon_{j0}^V + \sigma_{j0}^V)\delta\varepsilon_j^V \\ &+(\eta_j^{B_1}\overline{Er^{BV}}\Delta\varepsilon_{j0}^{B_1} + \sigma_{j0}^{B_1})\delta\varepsilon_j^{B_1} \\ &+(\eta_j^{B_2}\overline{Er^{BV}}\Delta\varepsilon_{j0}^{B_2} + \sigma_{j0}^{B_2})\delta\varepsilon_j^{B_2}\end{aligned} \tag{9}$$

On the other hand, the virtual strain energy δU stored in a concrete element is expressed as follows.

$$\delta U = \delta\varepsilon_X\sigma_X + \delta\varepsilon_Y\sigma_Y + \delta\gamma_{XY}\tau_{XY} \tag{10}$$

where $(\sigma_X, \sigma_Y, \tau_{XY})$ and $(\varepsilon_X, \varepsilon_Y, \gamma_{XY})$ are the stresses and strains with respect to *X* and *Y* coordinate system. Equating the virtual strain energy δU stored in the concrete element to the total one δU_L stored in the struts, we can obtain the incremental constitutive equations as follows.

$$\begin{Bmatrix}\sigma_X \\ \sigma_Y \\ \tau_{XY}\end{Bmatrix} = \begin{bmatrix}D_{11} & D_{12} & D_{13} \\ & D_{22} & D_{23} \\ sym. & & D_{33}\end{bmatrix}\begin{Bmatrix}\Delta\varepsilon_X \\ \Delta\varepsilon_Y \\ \Delta\gamma_{XY}\end{Bmatrix} + \begin{Bmatrix}\sigma_{X0} \\ \sigma_{Y0} \\ \tau_{XY0}\end{Bmatrix} \tag{11}$$

where D_{ij} are the stiffness matrix of element and σ_{X0}, σ_{Y0} and τ_{YX0} are the initial stresses at the stage of $\varepsilon_X, \varepsilon_Y$, and $\gamma_{XY} = \gamma_{YX}$. (The details of the components of the matrix are described in reference (Kato *et al.*, 1998).)

2.1.2 Equivalent Initial Stiffness for Each Strut Composing the Lattice Model

By assuming that the elastic constitutive equations are identical to the constitutive equations under plane stress condition of an isotropic elastic body, we can obtain here the equivalent initial stiffness for each strut composing the Lattice Model. In such a case of $\eta = 1$, the equivalent initial stiffness of hub struts, horizontal struts of ring element, and vertical and two bracing struts of ring element, is represented by $\overline{Er}$, $\overline{Er^H}$ and $\overline{Er^{BV}}$ respectively.

$$\overline{Er} = \frac{E}{6(1-\nu)} \tag{12}$$

$$\overline{Er^H} = \left[1 - \frac{2\sin^2\phi\cos^2\phi}{1+2\sin^4\phi}\left\{\frac{3(1-3\nu)}{2(1+\nu)}\right\}\right]\overline{Er} \tag{13}$$

$$\overline{Er^{BV}} = 1 - \frac{\tan^2\phi}{1+2\sin^4\phi}\left\{\frac{3(1-3\nu)}{2(1+\nu)}\right\}\overline{Er} \tag{14}$$

where E is the modulus of elasticity, and ν is a Poisson's ratio. In this paper, $f = 60°$ is assumed referring to the previous calculation (Kato *et al.*, 1996, 1997, 1998).

2.1.3 Stress-Strain Relations of Constitutive Struts

The stress-strain relations of hub struts, horizontal and bracing struts of the ring element are shown in Fig. 3(a), while the one for the vertical struts is shown in Fig. 3(b). The detail on how the hysteresis curves are defined was given in the references (Kato *et al.*, 1996, 1997, 1998). Briefly explaining, the values ($\sigma_c, \sigma_t, \varepsilon_{cul}, \varepsilon_{tul}, \varepsilon_0$ etc.) in Fig. 3(a) of the hub struts, horizontal and bracing struts are calculated based on the material properties (f_c, f_t, ε_c) of standard cylinder test. These values are determined mainly considering deformations under equibiaxial stresses. On the other hand, the compressive and tensile strength σ_t^V for the vertical strut of the ring element shown in Fig. 3(b) can be estimated mainly based on shear deformation, because the vertical strut can not resist equibiaxial stress conditions. Since the vertical strut of ring element is assumed mainly to resist against shear stress, the stress-strain relation for the vertical strut in the ring element is defined to be anti-symmetric. In Fig. 3(a), R_e and ε_{cul} are assumed to be 0.2 and $4\varepsilon_0$, respectively based on Darwin Model (Darwin *et al.*, 1976). The equation proposed by Saenz (Saenz, 1976) is adopted from the neutral O until the compressive strength P. After the compressive strength

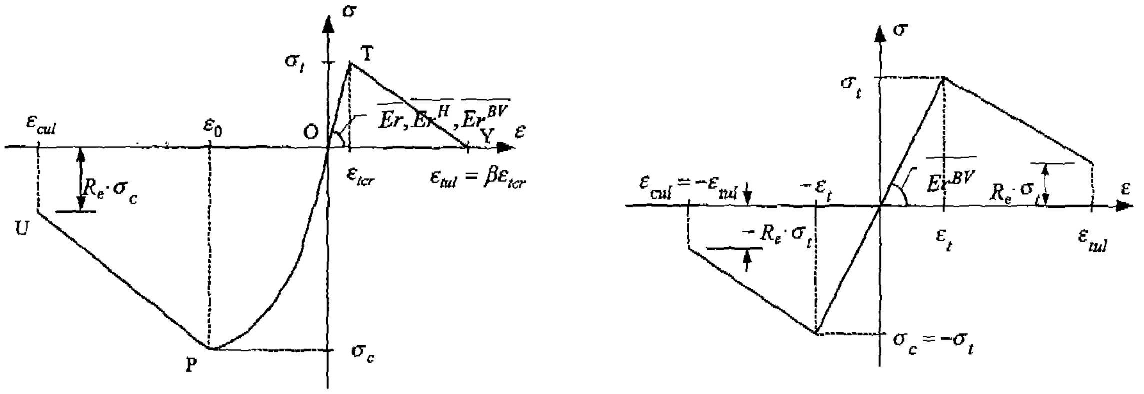

Fig. 3. Stress-Strain Relations of Constitutive Struts in the Lattice Mode. (a) Hub Strut, Horizontal and Bracing Strut of Ring Element, (b) Vertical Strut of Ring Element.

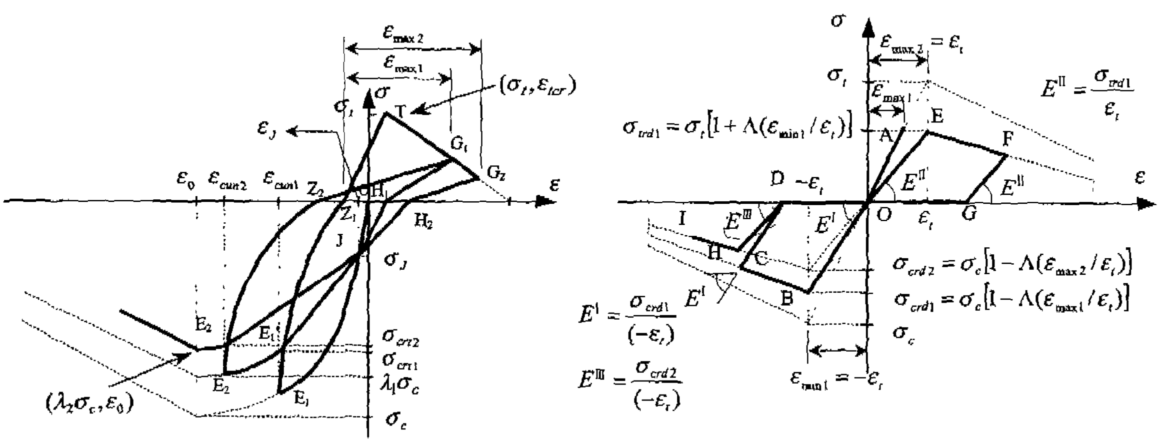

Loading Pass : O → E_1 → Z_1 → T → G_1 → H_1 → J → E_1 → E_2 → Z_2 → G_1 → G_2 → H_2 → J → E_2

J : the switchover point from tensile unloading curve to compressive enveloped curve

E': the return point on the compressive enveloped curve depending on the renewal maximum tensile strain ε_{max}

Loading Pass : O → A → O → B → C → D → O → E → F → G → O → D → H → I

The maximum value of ε_{max} is equal to ε_t.

And, the minimum value of ε_{min} is equal to $-\varepsilon_t$.

(a) (b)

Fig. 4. Stress-Strain Relations under Cyclic Loading. (a) Hub Strut, Horizontal and Bracing Strut of Ring Element, (b) Vertical Strut of Ring Element.

P, the straight degradation line, which connects P with U, is adopted. Generally, concrete elements may not resist against the tensile stress, after cracks arise in the concrete. However, the cracked concrete pretends to resist against tensile stress caused by a dowel action and an interlocking phenomena. In the present study, the tension stiffening factors β shown in Fig. 3(a) is assumed to be 2.0 from parametric studies (Kato *et al.*, 1996, 1997, 1998).

2.1.4 Cyclic Behavior of Struts Reflecting the Reduction Factor of Compressive Strength

The stress-strain relations of concrete elements if compressed excessively may degrade under cyclic loadings and the relations behave as shown in Figs. 4(a) and (b). In the present Lattice Model, the Modified Compression-Filed (Vecchio *et al.*, 1986) is adopted. The strain of plasticity ε_{cp} at the point Z is calculated by the equation proposed by Buyukozturk (Buyukozturk *et al.*, 1984). We adopt a circular curve for unloading. The straight line, which connects the point R with the point E, is adopted as a reloading curve. Therefore, the compressive strength of $\lambda\sigma_c$ pre-cracked concrete is reduced depending on the maximum tensile strain ε_{max} ever experienced.

$$\lambda = 1 - \Lambda\frac{\varepsilon_{max} - \varepsilon_{tcr}}{\varepsilon_{rd} - \varepsilon_{tcr}} \tag{15}$$

where $\varepsilon_{rd} = \varepsilon_{tcr} + \kappa(\varepsilon_{tcr} - \varepsilon_{cp})$, $\kappa = 2.7$.

The reduction rate of the strength in cracked concrete may be determined by the roughness of the crack surface but limited only to the neighborhood of cracks. The values of the reduction factor are assumed to have a minimum limit $1.0-\Lambda$ shown in Fig. 5 (Izumo *et al.*, 1989). The reduction factors Λ of the struts assumed in the Lattice Model are shown in Table 1 referring to the previous calculations (Kato *et al.*, 1997, 1998). When the cracked concrete element is subjected to a compression strain, the cracks close again. For expressing such a stress degradation, a switchover point as depicted as in σ_j Fig. 4(a) is

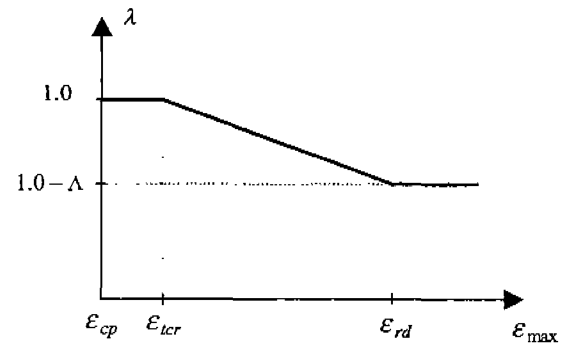

Fig. 5. Reduction Factor of Compressive Strength (Izumo *et al.*, 1989).

Table 1. Reduction Factor Λ (Kato *et al.*, 1997,1998) and Switchover Factor ς (Naganuma *et al.*, 2000)

Strut Name	Reduction Factor Λ	Switchover Factor ς
Hub Strut	$\Lambda^{hub} = 0.4$	$\varsigma^{hub} = 0.1$
Vertical Strut of Ring Element	$\Lambda^{V} = 0.4$	$\varsigma^{V} = 0.0$
Horizontal Strut of Ring Element	$\Lambda^{H} = 0.0$	$\varsigma^{H} = 0.5$
Bracing Struts of Ring Element	$\Lambda^{B1}, \Lambda^{B2} = 0.8$	$\varsigma^{B1}, \varsigma^{B2} = -2.0$

assumed based on the study by Naganuma (Naganuma *et al.*, 2000). These switchover points and the recent maximum strength being renewed step by step are connected by polygonal line. The value of the stress σ_J for the switchover point J is assumed as ς time the tensile strength based on Naganuma Model shown in Table 1. The compressive strength and tensile strength for vertical struts of the ring element in Fig. 4(b) are reduced by the maximum tensile strain ε_{max} and the minimum compressive strain ε_{min} ever experienced, respectively.

$$\lambda_t = 1 + \Lambda\frac{\varepsilon_{min}}{\varepsilon_t},\ \lambda_c = 1 - \Lambda\frac{\varepsilon_{max}}{\varepsilon_t} \tag{16}$$

2.2 Stress-Strain Relations of Steel Reinforcements

The reinforcing steels placed orthogonally within walls are approximated by two steel sheets, which resist uni-axially with a bi-linear type stress-strain relation as shown in Fig. 6. The steel elements are assumed to effectively work equally against both tension and compression.

2.3 Definition of Concrete Cracks

The Lattice Model represents a stress condition using combination of many straight struts. However, the definition of cracks as a continuum cannot be determined

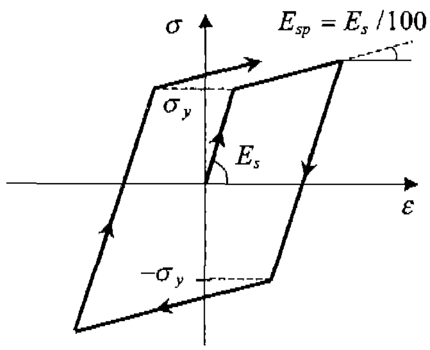

Fig. 6. Stres-Strain Relations for Reinforcing Steel.

directly by using the cracks of those struts. Accordingly, the generation of cracks in concrete is defined in this study as a condition under which the principal tensile strain calculated by the strains $(\varepsilon_X, \varepsilon_Y, \gamma_{XY})$ at an integration point exceeds the tensile limit strain. The tensile limit strain is assumed as follows.

$$\varepsilon_1^{Crack} = \lambda_{crack}\frac{f_t}{E_c} \tag{17}$$

where λ_{crack} is assumed to be 2.0 in the present analysis. f_t and E_c are respectively the tensile strength for cylinder test and the Young's Modulus.

2.4 Incremental Scheme

To investigate the RC shear wall responses, the displacement incremental scheme is used for analyzing the nonlinear behavior and for avoiding the numerical instability caused by the sudden changes of the stress states due to concrete cracks.

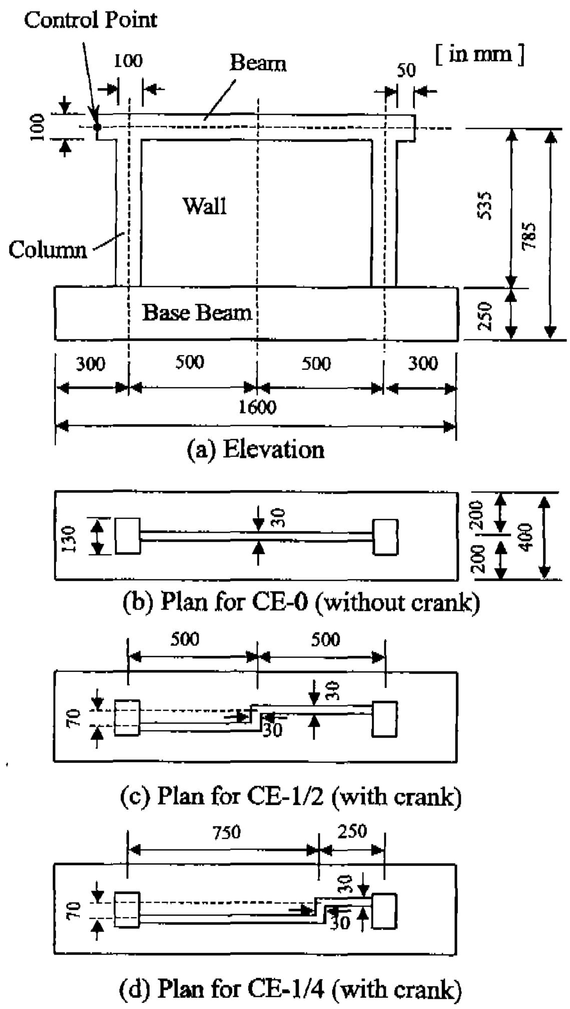

Fig. 7. Shapes and Dimensions of RC Shear Walls.

3. Experiment

Three specimens (Takayama *et al.*, 2000), designated CE-0, CE-1/2 and CE-1/4, are shown in Fig. 7. The crank position is summarized for each wall in Table 2, which also gives the material properties for each of the specimens. All three specimens were of 1,000 mm span, 535 mm height and 30 mm thickness, and reinforced by a common RC frame with 100×130 mm section. The thickness of the walls was designed 30 mm, however, the real thickness of each wall was actually a little thicker than the designed value as shown in Table 2. Fig. 8 shows the arrangement of reinforcement steels of the typical wall (CE-0). Single-layer reinforcement steels (diameter=2.5 mm) were arranged orthogonally in the wall. The cyclic horizontal loads were applied statically to the specimens. The peak of each cycle was controlled by displacement at

Table 2. Material Properties of the Models, Concrete and Reinforcements

			CE-0	CE-1/2	CE-1/4
Model	Position of crank		None	Center	Quarter
	Thickness of Wall	[mm]	31.44	31.10	31.53
	Ratio of Reinforcements	[%]	0.409	0.409	0.409
Concrete	Compressive Strength	[N/mm²]	39.1	33.1	36.8
	Tensile Strength	[N/mm²]	3.37	2.89	3.42
	Young's Modulus	[kN/mm²]	24.4	23.6	24.8
	Poisson's Ratio		0.166	0.179	0.181
Reinforcement			ϕ2.5	D10	
	Young's Modulus	[kN/mm²]	216	201	
	Yield Strength	[N/mm²]	639	393	
	Ultimate Strength	[N/mm²]	675	508	

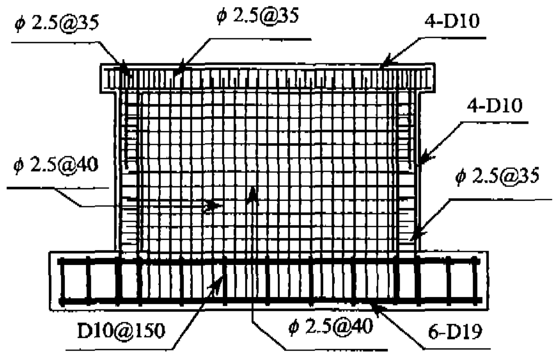

Fig. 8. Reinforcement Arrangement (CE-0).

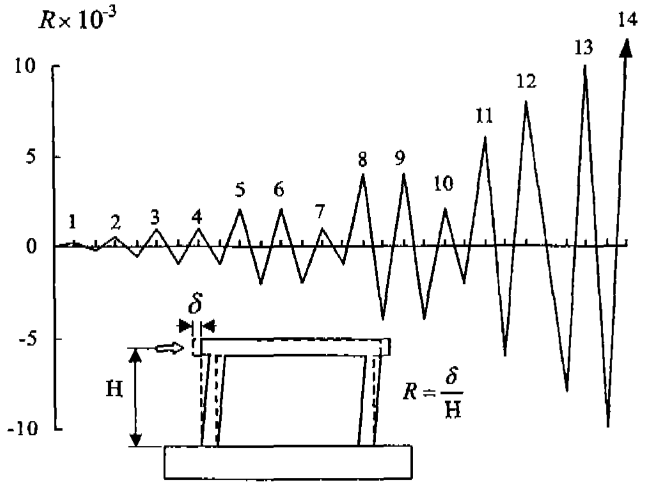

CYCLE	$R(\times10^{-3})$
1	0.25
2	0.50
3	1.00
4	
5	2.00
6	
7	1.00
8	4.00
9	
10	2.00
11	6.00
12	8.00
13	10.0
14	Failure

Fig. 9. Procedure of Cyclic Loading.

the top of the wall. The procedure of cyclic loadings is shown in Fig. 9. In 14th cyclic, the loads were applied increasingly until the failure of the specimen.

4. Numerical Analysis

The numerical models, CE-0, CE-1/2 and CE-1/4, are divided with shell elements, respectively as shown in Figs. 10(a), (b) and (c). In the CE-0 model, the wall is divided into 6×10 elements. In the CE-1/2 and CE-1/4 models, the walls are divided into 6 elements in the vertical direction and into 12 and 13 elements considering cranks in the hor-

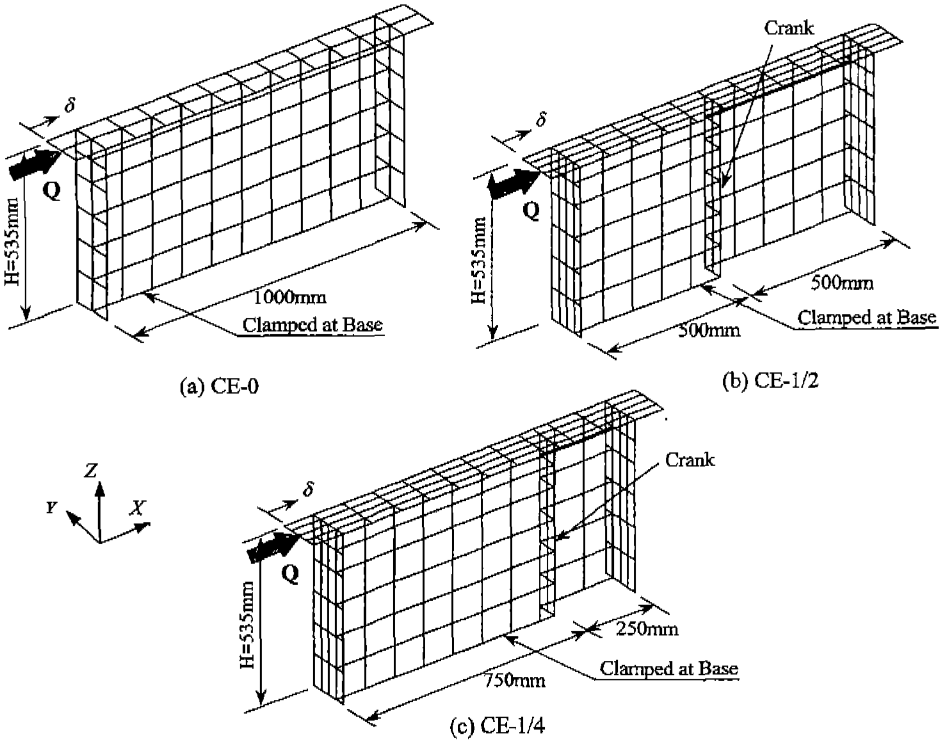

Fig. 10. Finite Element Mesh.

izontal direction, respectively. Then, each column is divided into 6 elements in the vertical direction. The beam at the top is divided into 12 elements for CE-0 and CE-1/2 models, and 13 elements for CE-1/4 model in the horizontal direction. Also, the column and beam are divided in the *Y* (lateral) direction into 2 elements for CE-0 model and 4 elements for CE-1/2 and CE-1/4 models as shown in Fig. 10.

Within each shell element for the walls is divided into 8 concrete layers and 2 steel layers, and every element for beams and columns is divided into 8 concrete layers and 4 steel layers. In the numerical model, the designed shell thickness (t=30 mm) is adopted for walls. The reinforcing ratios of the wall in both vertical and horizontal direction are 0.409% in the all specimens. The reinforcements in the wall are arranged at center through thickness. The concentrated loads at each node in the loading beam are applied. In the numerical analysis, the displacement control is adopted while all the horizontal displacements of the loading beam are assumed same in the *X* direction.

5. Comparison Between Numerical and Experimental Results

Figs. 11(a), (b) and (c) show the load Q(kN)- displacement δ(mm) relations for CE-0, CE-1/2, CE-1/4, respectively. The solid lines denote the numerical responses, and the solid lines with filled diamond marks denote the experimental ones in the each specimen. Fig. 11(d) shows the ratio of the ultimate shear strength. The ultimate load Q_{ult} and the load at R=1/100 are listed in Table 3 and the ultimate shear strength is non-dimen-sionalized by the following Eq. (18).

$$\chi = \frac{n_{ult}}{f_c'} = \frac{Q_{ult}}{A_w f_c'} \tag{18}$$

where Q_{ult}, A_w and f_c' respectively the ultimate load, the cross section of the horizontal wall section and the com-

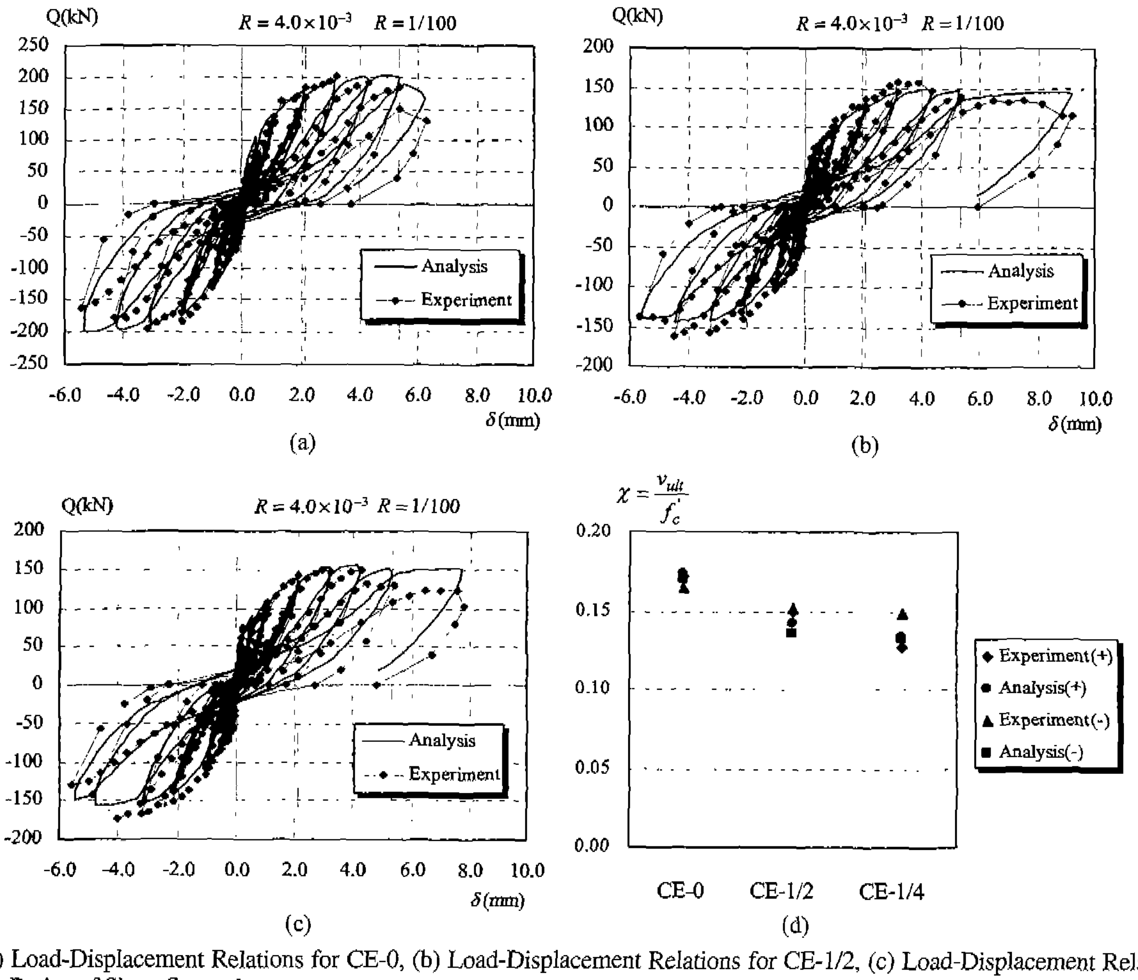

Fig. 11. (a) Load-Displacement Relations for CE-0, (b) Load-Displacement Relations for CE-1/2, (c) Load-Displacement Relations for CE-1/4, (d) Ratios of Shear Strength.

Table 3. List of Loading

Horizontal Loading Q (kN)		CE-0		CE-1/2		CE-1/4	
		(+)	(−)	(+)	(−)	(+)	(−)
Ultimate Load $Q\ ult$ [kN]	Experiment	201.9	192.9	158.3	161.4	150.5	174.3
	Analysis	203.4	199.8	150.5	144.6	157.2	156.2
	Ex/An	0.99	0.97	1.05	1.12	0.96	1.12
Load of R=1/100 [kN]	Experiment	183.9	163.0	137.7	138.3	130.4	130.7
	Analysis	196.9	197.5	145.5	140.7	151.7	148.8
	Ex/An	0.93	0.83	0.95	0.98	0.86	0.88
Compressive Strength, f_c'	[N/mm²]	39.1		33.1		36.8	
$\chi = \frac{v_{vlt}}{f_c'} = \frac{Q_{ult}}{A_w f_c'}$	Experiment	0.172	0.164	0.149	0.152	0.127	0.148
	Analysis	0.173	0.170	0.142	0.136	0.133	0.132

Note: A_w [mm²] is the cross section of the wall part.

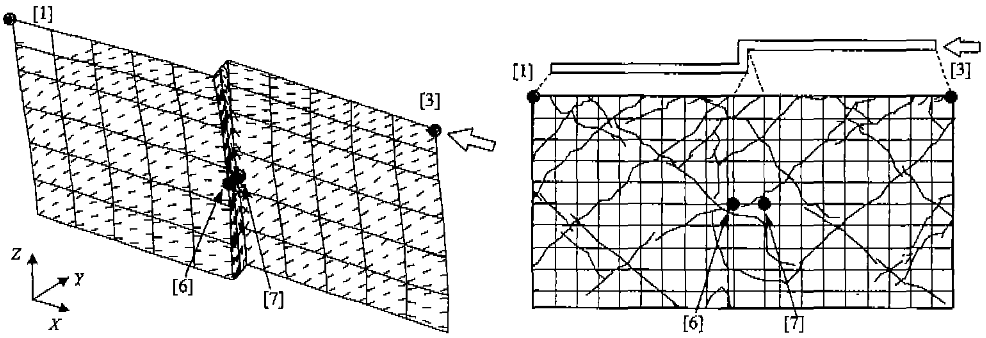

(a) (b)
(a) Analysis (Crack and Deformed Pattern) (b) Experiment (Crack Pattern)

Fig. 12. Crack and Deformed Pattern in the Wall Part for CE-1/2 at R=4.0×10⁻³ (Side A).

pressive strength as of cylinder test.

The ratio of experimental to numerical results of the ultimate load Q_{ult} falls from 0.96 to 1.12, and the ratio of those for R=1/100 (see Fig. 9; 13 cycles) ranges from 0.83 to 0.98 in Table 3. In Figs. 11(a), (b) and (c) and Table 3, fine agreements are obtained between the numerical and experimental results with respect to both of the ultimate load and areas of hysteresis loops while the hysteresis loops in the numerical responses are a little smaller than the experimental ones. And the ductile deformation and low carrying capacity for crank type shear wall are found, since relatively larger sway is produced for the crank typed walls. On the other hand, Fig.11(d) shows that the ultimate shear strength of the shear walls with a crank tends to decrease due to the presence of the crank at most by the order of 25% than those without cranks.

Figs. 12(a) and (b) show the crack pattern found within the wall of the model CE-1/2 for R=4.0×10⁻³ through both the numerical and experimental results. The deformed pattern for R=4.0×10⁻³ is also shown in Fig. 12(a). Comparison between the numerical and experimental results with respect to the deformation for CE-1/2 in each position as shown in Figs. 12(a) and (b) are listed in Table 4. In Figs. 12(a), (b) and Table 4, the deformations are globally in fine agreements between the numerical and experimental responses in the X and Y directions. And an almost same crack pattern with about 45-degrees angle is gen-

Table 4. The Deformation of Each Point for CE-1/2 at R=4.0×10⁻³ [mm]

No.	X direction		Y direction		Z direction	
	Ex	An	Ex	An	Ex	An
1	−2.03	−2.13	−0.11	0.00	0.12	0.10
3	−2.13	−2.13	−0.90	0.00	0.67	0.63
6	0.28	−0.48	−0.10	−0.13	0.98	0.54
7	−1.13	−1.50	0.64	0.29	−0.25	0.19

erated, however, a difference of deformation near the crank is observed between the numerical and experimental responses. Judging globally, not only the ultimate load but also the total behavior of deformation of the shear walls under cyclic loading may be simulated based on the Lat-tice Model.

6. Conclusions

In this paper, the cyclic behavior of the shear walls with and without crank is examined both numerically and experimentally. The conclusions are drawn as follows.

1. The validity and applicability of the constitutive equations based on the Lattice Model *A* for RC shear walls with and without crank subjected to cyclic loading is confirmed.
2. In the present numerical analysis, the ductile deformation is found with a little smaller shear strength for crank type shear walls as depicted in the experiment.
3. Similarly to other numerical results of walls, it is confirmed that the reduction factors for the compressive strength is necessary for simulating cyclic behaviors.

Acknowledgement

The authors express sincere appreciation to many students of Takayama Laboratory in the Kanazawa Institute of Technology who performed the experiment for this study.

References

Buyukozturk O, Ming TT (1984) Concrete in biaxial cyclic compression, Journal of Structural Engineering, 110(3): 461-476.

Darwin D, Pecknold DA (1976) Analysis of RC shear panels under cyclic loading, Proceedings of the ASCE, 102(ST2): 355-369.

Hinton E, Owen DRJ (1984) Finite Element Software for Plates and Shells, Pineridge Press, Swansea, UK.

Izumo J, Shin H, Maekawa K, Okamura H (1989) Analytical model for a reinforced concrete panel element subjected to reversed cyclic in-plane stresses, Journal of Materials, Concrete Structures and Pavements, 408: 51-60 (in Japanese).

Kato S, Mutoh A, Maeda S (1996) A concept of lattice model for inelastic constitutive equation of reinforced concrete shells under cyclic loading and application to FEM, Proceedings of The 3rd Asian-Pacific Conference on Computational Mechanics, Seoul, Korea: 1417-1422.

Kato S, Ohya M, Maeda S (1997) A new formulation of constitutive equations for reinforced concrete element based on lattice model and application to FEM analysis of reinforced concrete shells, Proceedings of 5-th International Conference on Computational Plasticity, Barcelona, Spain.

Kato S, Ohya M, Maeda S, Yoshino F (1998) The formulation of constitutive equation for concrete based on the ring typed-latticed model and its application to finite element analysis of reinforced concrete shells, Journal of Structural Engineering, 44B: 441-454 (in Japanese).

Naganuma K, Ohkubo M (2000) An analytical model for reinforced concrete panels under cyclic stresses, Journal of Structural and Construction Engineering, AIJ, 536: 135-142 (in Japanese).

Saenz LP (1976) Discussion of equation for the stress-strain curve of concrete by desayi and krshman, Journal of ACI, 61: 1229-1235.

Takayama M (1990) Elasto-plastic characteristics of reinforced concrete folded wall subjected to lateral forces, Proceedings of the Third Summer Colloquium on Shell and Spatial Structures: 269-277.

Takayama M, Fujita K (2000) Elasto-plastic behavior of crank type reinforced concrete shear walls, Proceedings of Sixth Asian Pacific Conference on Shell and Spatial Structures: 485-492.

Vecchio FJ, Collins MP (1986) The modified compression-field theory for reinforced concrete elements subjected to shear, ACI Journal, Proceedings 83(2): 219-231.